*Original Research Article*

# Structural and Magnetic Properties of Nano Cu-Zn-Zr Ferrite for Magnetic Temperature Transducer (MTT).


## Abstract

$Cu_{1-x}Zn_{x+y}Zr_yFe_{2-2y}O_4$ (Cu-Zn-Zr ferrite) series of compositions with x= (zero, 0.4, 0.6, 0.8, 1) when y= (0.05, and 0.1) nanoparticles were synthesized using citrate sol-gel method. The prepared nanoparticles were characterized by X-ray diffraction (XRD) and transmission electron microscopy (TEM). Lattice parameter, bulk density, theoretical density, and porosity were measured for (Cu-Zn-Zr ferrite) samples. The XRD pattern indicated that the average crystallite size found from 18-30 nm and from 17-24 nm, while the average particle size from TEM images are ranging from 21-39 nm and from 18-24 nm for y= (0.05 and 0.1) respectively. Magnetic hysteresis loop measurements illustrate that materials exhibit as soft ferrite at low Zn contents, while at higher Zn contents all materials behave as superparamagnetic materials without any saturation magnetization Ms. The initial magnetic permeability ($\mu_i$) at two frequencies 1 KHz and 10 KHz as a function of temperature was measured. A sudden change in $\mu_i$ appear around Curie temperature, making our samples good candidates for Magnetic Temperature Transducer (MTT) devices.


**Keywords:** Cu-Zn-Zr ferrite, nanoparticles, MTT, XRD, FTIR, SEM, EDX, VSM, magnetic hysteresis loop, Magnetic properties, magnetic permeability, saturation magnetization, and citrate sol-gel method.

# 1. Introduction

Over recent decades, nanomaterials represent a great importance because of their unique physical and chemical properties which completely different from their bulk counterparts, and their most important advantage is the miniaturization of particle size. It is known that the preparation method affecting on the effective parameters of ferrites such as magnetization, initial permeability, Curie temperature, and structural properties. Cu-Zn-Zr ferrite nanoparticles possesses important magnetic properties for several advanced technological, industrial, catalytically, and electrical applications e.g. magnetic recording devices, high quality filters, magnetic resonance imaging enhancement, storage devices, microwave devices, power transformers, electric generators…etc. [1-4].

Ferrites have the general formula of $MFe_2O_4$ (where M (divalent metallic ion): Fe, Co, Ni, Cu, Mg, etc.,) and a unit cell contains 32 O-atoms in a cubic close packing with 8 (tetrahedral) (A site) and 16 (octahedral) (B site) occupied sites. In most ferrite materials, the substituents play an important role in determining the variation of the physical properties. The substitution can be divided into the following types: direct replacement of $Fe^{+3}$ on tetrahedral (A) or octahedral (B) sub lattice by the substituent ion, with consequential redistribution of $Fe^{+3}$ ions between A and B sub lattices which lead to the change of ferromagnetic spin structure. The extent of iron redistribution depends on the specific nature of the substituting ion [5, 6].

By virtue of their magnetic and semiconducting properties, the copper ferrites and its compositions with other ferrites are employed as magnetic materials for multiplayer chip inductors but also for transducers of high thermo-magnetic sensitivity [7]. Currently, a new type of temperature-sensitive element using for construction of devices for controlling temperature. The sudden change of initial magnetic permeability near Curie temperature represent the main factor to using such element [3]. Many researchers was reported the substitution of different elements such as Co [8], Ni [9-11] and Tb [12] in ferrites to enhance their magnetic and electrical properties [13].

Presently, various physical and chemical techniques have been developed to prepare nanomaterials. The chemical techniques for the synthesis of nanostructured materials offer some advantages in comparison with the physical techniques in relation to simplicity, energy saving and product homogeneity[5]. The widely used chemical methods are co-precipitation [14], hydrothermal [15], electro deposition [16], micro-emulsion [17], auto-

combustion [18], sucrose method [19], reverse micelle [20],and Citrate Sol-Gel technique [21, 22].

Among these methods, the citrate-gel method can be used to prepare nanocomposite of spinel ferrites with specific properties, such as controlled stoichiometry and narrow particle size distribution. The cheapness, simplicity of experimental set-up, short time of production and the purity and homogeneity of final product are the most important features that distinguish this technique. In addition, the speed and low temperature of the synthesis process prevent the sintering of the obtained samples; which confirms that this technique is special compared with other synthesis techniques [23].

This paper aims to study the substitution influence of Zn and Zr on structure, microstructure, and consequently, magnetic properties of Cu ferrite.

# 2. Experimental

## 2.1 Materials:

The starting materials for the citrate precursor synthesis route were $Cu(NO_3)_2.3H_2O$, $Fe_2(NO_3)_3.9H_2O$, $Zn(NO_3)_2.6H_2O$, $ZrOCl_2.8H_2O$ and citric acid ($C_6H_8O_7$) were of analytical grade.

## 2.2 Synthesis of Cu-Zn-Zr ferrite nanocomposites:

The samples were prepared by sol-gel method and was annealed at 800℃. The first step is the formation of complex compounds (chelates) between polybasic citric acid and various metal cations. In typical procedure, the stoichiometric amounts of cupper nitrate, ferric nitrate, zinc nitrate, and zirconium oxychloride were taken in a glass beaker and dissolved in de-ionized water. The compositions of the Zn and Zr-substituted $CuFe_2O_4$ were represented by $Cu_{1-x}Zn_{x+y}Zr_yFe_{2-2y}O_4$ with x= (zero, 0.4, 0.6, 0.8, 1) when y= (0.05, and 0.1). The solution was heated on a hot plate up to 60 ℃ then citric acid was added. The metal nitrates: citric acid molar ratio was fixed at 1:1. The citrate–nitrate mixture was heated and vigorously stirred with magnetic stir bar at 90 ℃ until a gel was formed. The resulting gel was placed in a drying oven at 105 ℃ for 24 hours. The dried gel was crushed using an agate mortar and transformed into muffle furnace then fired at 800 ℃ in alumina crucibles.

### 2.3 Characterization of Cu-Zn-Zr ferrite nanocomposites:

The X-ray diffraction (XRD) of nanocomposites was carried out at room temperature using (APD 2000 pro, H423-virtical diffractometer) equipped with Cu Kα radiation (k = 1.540598 Å). The particle size and morphology of nanocomposites were investigated by JEOL JEM-2100 transmission electron microscopy (TEM). The TEM specimen was prepared by the ultrasonic dispersion of small amount of the powders in a few milliliters of ethanol, and then dropping on a copper grid covered in an amorphous carbon film.

## 3. Results and discussion

### 3.1 X-Ray Diffraction Studies:

***Fig.1. (a)*** and ***(b)*** shows the indexed X-Ray different pattern of Cu-Zn ferrite doped with Zr ions with mole content 0.05 and 0.1 respectively. The diffraction pattern confirm the formation of single-phase panel structure without presence of foreign peaks especially at high Zn content. At low value of Zn content, some peaks belong to other phases are present which disappear at high Zn content. This indicates the role that Zn ion plays as a catalyst for speeding the solid-state reaction and the formation of single phase. The particle size was calculated from the most intense peaks [(220) (311) (511) (440)] by using Scherer's equation [24]:

$$D = \frac{K\lambda}{\beta \cos\theta}$$

Where K is the Scherer's constant and equal 0.89. The value of K depends on several factors including the Miller indices of the reflection plane and the shape of phase crystal. If the shape is unknown K often assigned of 0.89, λ is the wavelength of the X-ray for Cu-Kα (λ =1.540598Å), θ is the diffraction angle and $\beta$ is the full width at half maximum (FWHM) in radian.

***Table.1*** shows that the crystallite size (**D**) decrease for both series (y=0.05 and 0.1) above x=0.4 by increasing $Zn^{2+}$ content then increase at x=1. The value of lattice constant ($a$) increase by increasing Zn content for $Zr^{4+}$ ion = 0.05 and 0.1. When a cation whose radius and valance are differ from those of the host cations is introduced into the spinel lattice, a strain in the lattice is created while affect the unit cell dimensions.

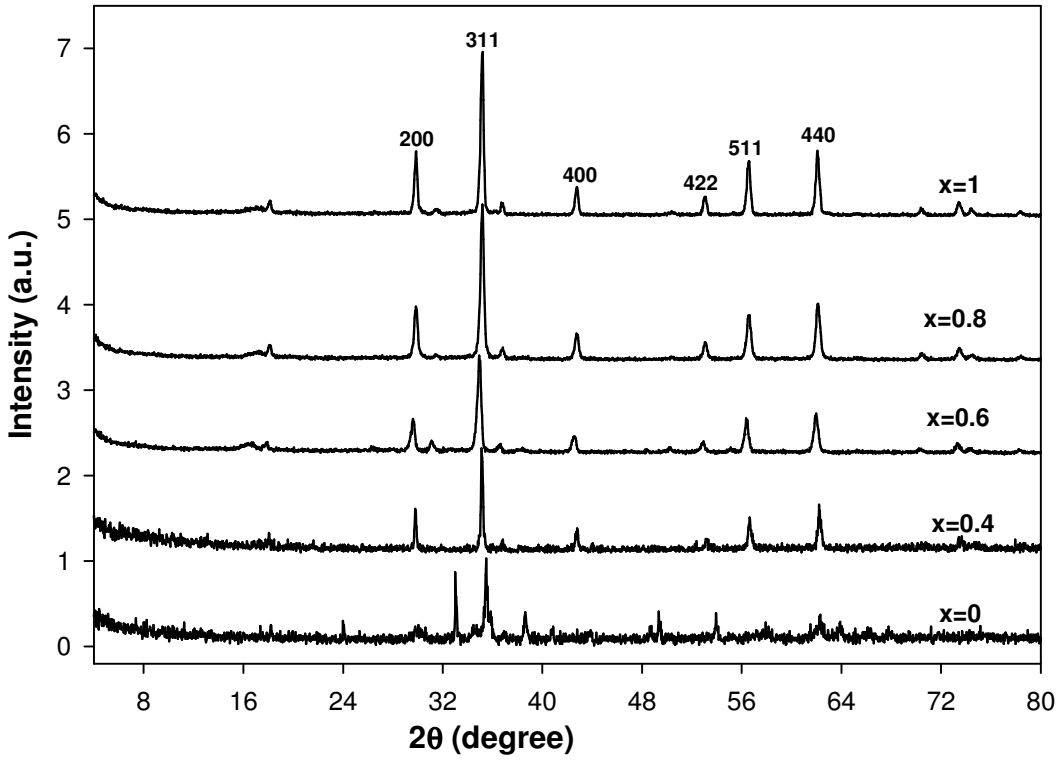


**(a)**

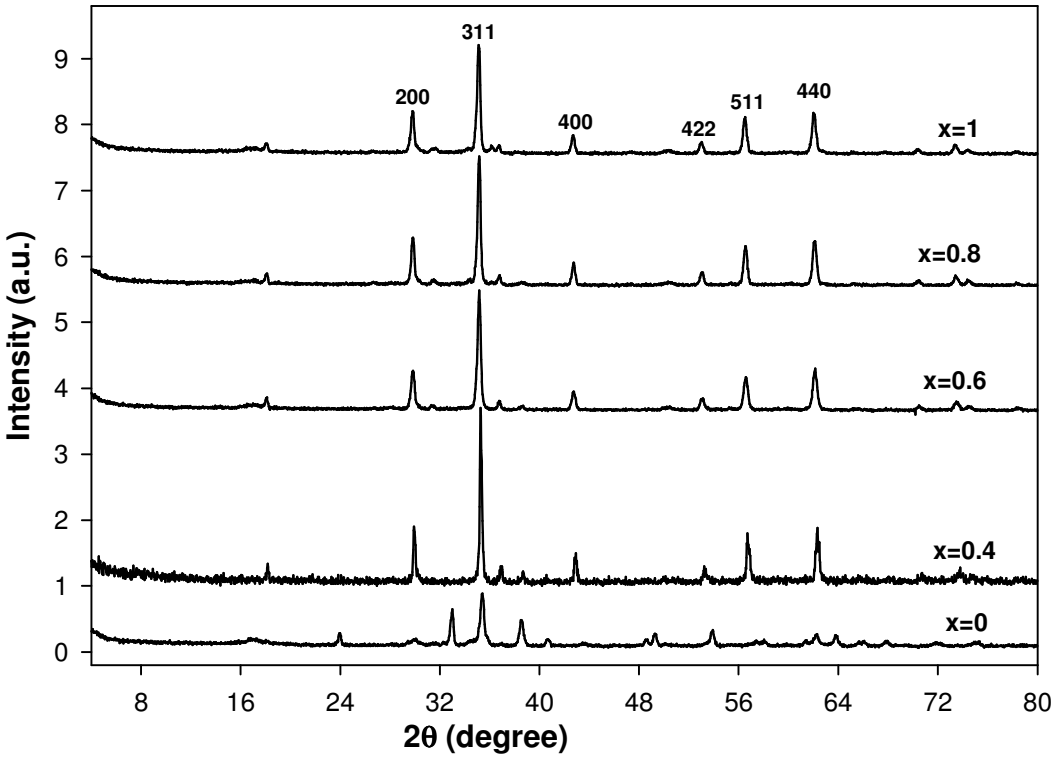


**(b)**

**Fig.1:** The XRD patterns of the prepared $Cu_{1-x}Zn_{x+y}Zr_yFe_{2-2y}O_4$ where x= (zero, 0.4, 0.6, 0.8, 1), **(a)** y=0.05, and **(b)** y= 0.1.

**Table.1**: The structural parameters of (Cu-Zn-Zr) ferrite samples.

| Y | x | Lattice parameters | | Crystallite size D (nm) | Cell volume $V_{exp}$ (Å)$^3$ |
|---|---|---|---|---|---|
| | | $a_{th}$ (Å) | $a_{exp}$ (Å) | | |
| 0.05 | 0 | 8.37 | 8.39 | 29.9 | 590.6 |
| | 0.4 | 8.39 | 8.44 | 30.2 | 601.2 |
| | 0.6 | 8.4 | 8.50 | 20.8 | 614.1 |
| | 0.8 | 8.41 | 8.51 | 18.7 | 616.3 |
| | 1 | 8.41 | 8.44 | 23.2 | 601.2 |
| 0.1 | 0 | 8.39 | 8.39 | 19.4 | 590.6 |
| | 0.4 | 8.41 | 8.41 | 24.1 | 594.8 |
| | 0.6 | 8.42 | 8.42 | 17.6 | 596.9 |
| | 0.8 | 8.426 | 8.43 | 17.6 | 599.1 |
| | 1 | 8.431 | 8.46 | 19.7 | 605.5 |

The ionic radii of $Zn^{2+}$ ions 0.74(Å) and $Zr^{4+}$ ions 0.79(Å) are larger than that of $Fe^{3+}$ ions 0.64(Å), the lattice seems to expand likely to accommodate the increasing number of $Zn^{2+}$ and $Zr^{4+}$ ions resulting into the increasing of lattice constant.

The measured density was calculated from the weight and dimension method and are shown in ***Fig.2.*** From this figure it is evident that, the measured density increase with Zn and Zr content in the lattice which may be attributed to the difference of ionic radii of $Zn^{2+}$, $Zr^{4+}$and $Fe^{3+}$. The presence of Zn ions enhance the grain growth due to the great solubility in the spinel phase at higher concentration.

The theoretical density of spinel phase were calculated from the following equation [25]:

$$D_x = \frac{8M}{Na^3} \ (g/cm^3)$$

Where M is the molecular weight,

N is the Avogadro's number, equal to ($6.022 \times 10^{23}$ $mole^{-1}$)

The theoretical density nearly remain constant by increasing Zn content and has larger value than bulk density due to the presence of pores in the material. The x-ray density increase with increasing Zn and Zr content, which is referred to the increase in molecular weight and lattice constant.

The porosity of the samples decrease with increasing Zn and Zr content due to the difference in ionic radii as shown in ***Fig.2.***

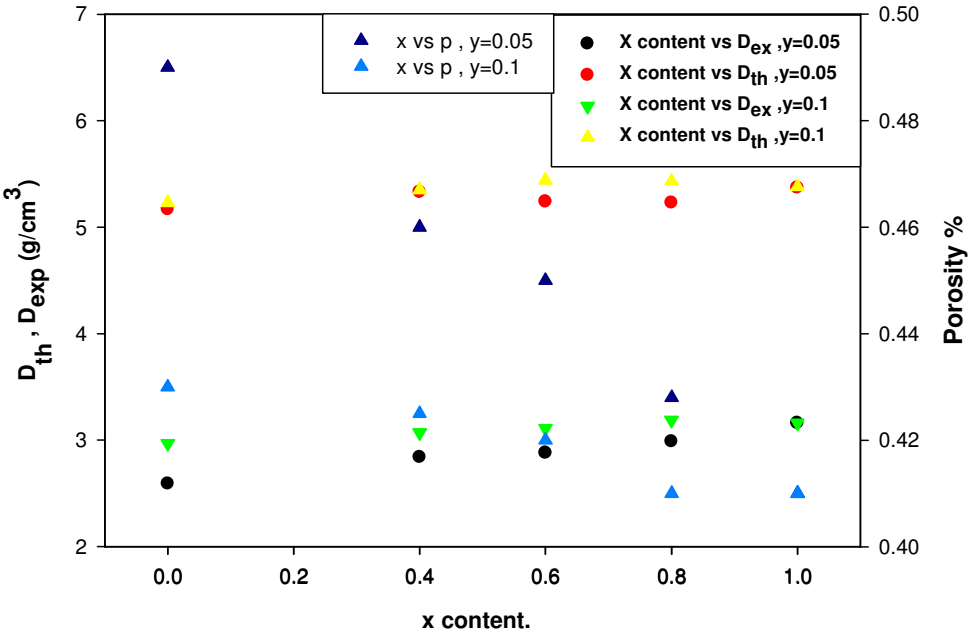


**Fig.2:** The porosity, theoretical density and bulk density with x contents for prepared samples.

***Fig.3.*** show the relation between the radius of tetrahedral (A-Site) and octahedral (B-Site) respectively for our samples. The radius of tetrahedral site $r_A$ decrease by increasing the Zn content while the radius of octahedral site $r_B$ increase. The substitution of $Zn^{2+}$ ions with radius 0.74Å instead of $Fe^{3+}$ ions leads to increase of $r_A$. The decrease of cation with radius 0.72Å at octahedral site leads to the decrease of $r_B$. The addition of $Zr^{4+}$ ions does not affect on the $r_B$ due to its small ratio.

The expected cation distribution of our samples may be given from the following formula:

$$(Zn_{x+y}\ Zr_{y-t}\ Fe_{1-x-2y+t}\ )[Cu_{1-x}\ Zr_t\ Fe_{1+x-t}\ ]$$

The theoretical lattice parameter can be calculated using the value of $r_A$, $r_B$ and $R_O$(radius of oxygen ion) from the following relation [26]:

$$a = \frac{8}{3\sqrt{3}}[(r_A+R_O) + \sqrt{3}(r_B+R_O)] \quad (Å)$$

To calculate $r_A$ and $r_B$, it is necessary to know the cation distribution which can represented by the above estimated equation at which the theoretical and experimental lattice parameter are co-inside. The expected cation distribution are given in ***Table.2***.

**Table.2**: Cation distribution for (Cu-Zn-Zr) ferrite samples.

| y | x | Chemical Structure | A-Site | B-Site |
|---|---|---|---|---|
| 0.05 | 0 | $Cu_1Zn_{0.05}Zr_{0.05}\mathrm{Fe}_{1.9}O_4$ | $(Zn_{0.05}Zr_{0.04}Fe_{0.91})$ | $\boldsymbol{[Cu_1Zr_{0.01}Fe_{0.99}]}$ |
| | 0.4 | $Cu_{0.6}Zn_{0.45}Zr_{0.05}\mathrm{Fe}_{1.9}O_4$ | $(Zn_{0.45}Zr_{0.04}Fe_{0.51})$ | $\boldsymbol{[Cu_{0.6}Zr_{0.01}Fe_{1.39}]}$ |
| | 0.6 | $Cu_{0.4}Zn_{0.65}Zr_{0.05}\mathrm{Fe}_{1.9}O_4$ | $(Zn_{0.65}Zr_{0.04}Fe_{0.31})$ | $\boldsymbol{[Cu_{0.4}Zr_{0.01}Fe_{1.59}]}$ |
| | 0.8 | $Cu_{0.2}Zn_{0.85}Zr_{0.05}\mathrm{Fe}_{1.9}O_{4]}$ | $(Zn_{0.85}Zr_{0.04}Fe_{0.11})$ | $\boldsymbol{[Cu_{0.2}Zr_{0.01}Fe_{1.79}]}$ |
| | 1 | $Cu_0Zn_{1.05}Zr_{0.05}\mathrm{Fe}_{1.9}O_4$ | $(Zn_1)$ | $\boldsymbol{[Zn_{0.05}Zr_{0.05}Fe_{1.9}]}$ |
| 0.1 | 0 | $Cu_1Zn_{0.1}Zr_{0.1}\mathrm{Fe}_{1.8}O_4$ | $(Zn_{0.1}Zr_{0.08}Fe_{0.82})$ | $\boldsymbol{[Cu_1Zr_{0.02}Fe_{0.98}]}$ |
| | 0.4 | $Cu_{0.6}Zn_{0.5}Zr_{0.1}\mathrm{Fe}_{1.8}O_4$ | $(Zn_{0.5}Zr_{0.08}Fe_{0.42})$ | $\boldsymbol{[Cu_{0.6}Zr_{0.02}Fe_{1.38}]}$ |
| | 0.6 | $Cu_{0.4}Zn_{0.7}Zr_{0.1}\mathrm{Fe}_{1.8}O_4$ | $(Zn_{0.7}Zr_{0.08}Fe_{0.22})$ | $\boldsymbol{[Cu_{0.4}Zr_{0.02}Fe_{1.58}]}$ |
| | 0.8 | $Cu_{0.2}Zn_{0.9}Zr_{0.1}\mathrm{Fe}_{1.8}O_4$ | $(Zn_{0.9}Zr_{0.08}Fe_{0.02})$ | $\boldsymbol{[Cu_{0.2}Zr_{0.02}Fe_{1.78}]}$ |
| | 1 | $Cu_0Zn_{1.1}Zr_{0.1}\mathrm{Fe}_{1.8}O_4$ | $(Zn_1)$ | $\boldsymbol{[Zn_{0.1}Zr_{0.1}Fe_{1.8}]}$ |

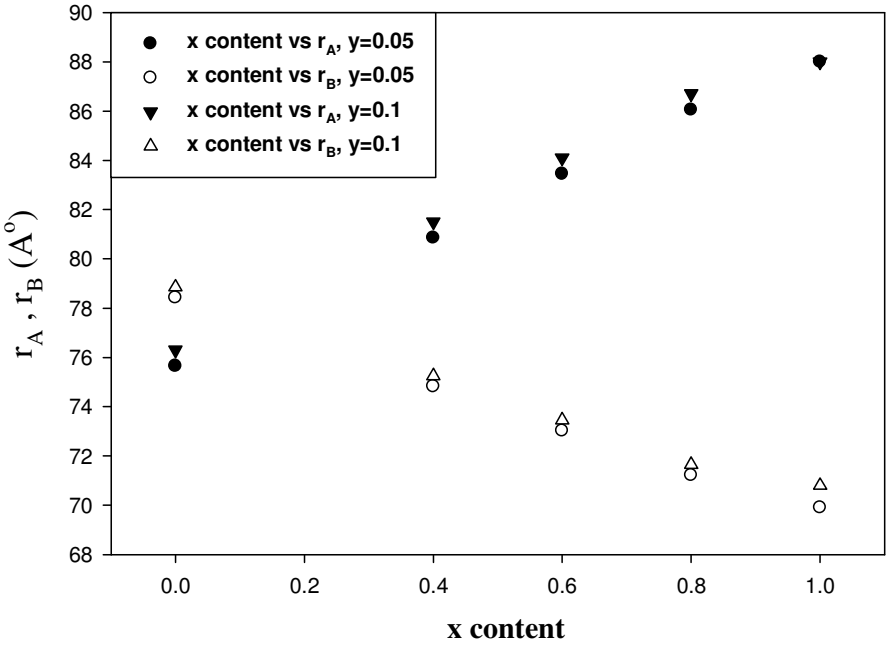


**Fig.3:** The radius of tetrahedral (A-Site) and octahedral (B-Site) for our samples.

## 3.2 The transmission electron microscopy (TEM):

The high resolution transmission electron microscope (HRTEM) was employed to confirm the results of XRD studies for all samples. ***Fig.4.*** shows the high crystallinity nature of the synthesized $Cu_{1-x}Zn_{x+y}\,Zr_y\;Fe_{2-2y}\;O_4$ nanoparticles at x=0.4 and y=0.1. The nanoparticles exhibit a cubic shapes where their diameter ranging from 17-39 nm with decreasing value by increasing Zn and Zr content. The crystallite size deduced from TEM varies near to that calculated from XRD as shown in ***Table.3***. The HRTEM for the studied samples have a lattice spacing which confirm the crystalline nature of the samples. The interplanner distance (d) was found to be 0.27 nm for x=0.4, y=0.1 which belong (220) plane. Other values of d spacing was 0.29 nm for x=0.6, y=0.05 which belong to (311) plane and 0.22 nm for x=0.6, y=0.1 that belong to (400) plane.

**Table.3**: The crystallite size deduced from TEM and XRD.

| y | x | D nm XRD | D nm TEM | (d) nm | Plane |
|---|---|---|---|---|---|

| | | | | | |
|---|---|---|---|---|---|
| 0.05 | 0.4 | 30.2 | 36.98 | — | — |
| | 0.6 | 20.8 | 33.22 | 0.27 | **(220)** |
| 0.1 | 0.4 | 24.1 | 28.06 | 0.29 | **(311)** |
| | 0.6 | 17.6 | 22.64 | 0.22 | **(400)** |

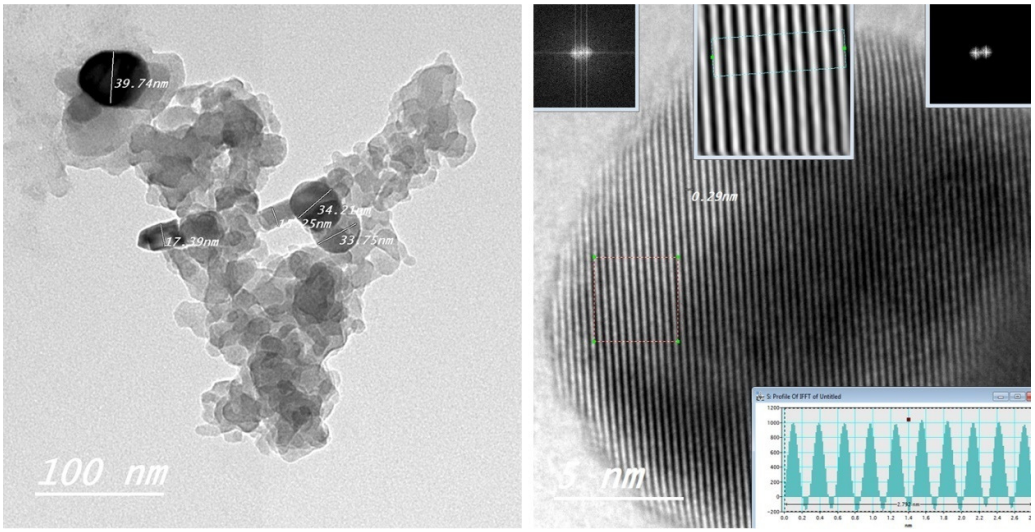


**(a)** **(b)**

**Fig.4: (a)** TEM image and **(b)** The (HRTEM) of $Cu_{0.6}Zn_{0.5}\,Zr_{0.1}\;Fe_{1.8}\;O_4$ sample.

## 3.3 Initial Magnetic Permeability:

The initial permeability ($\mu_i$) was measured at two frequencies 1KHz and 10KHz as a function of temperature for different Zn and Zr content which are shown in ***Fig.5.***

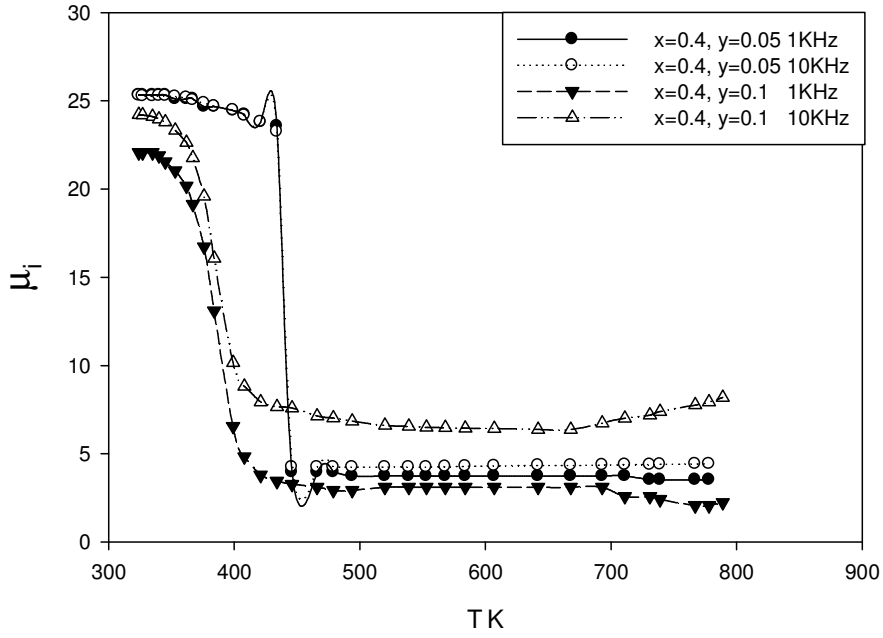


**(a)**

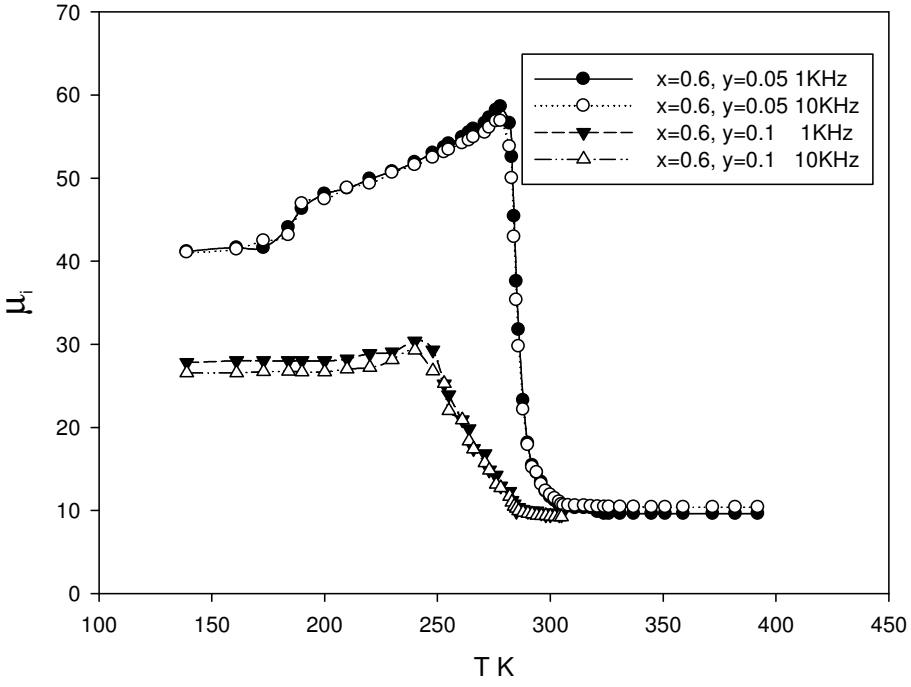


**(b)**

**Fig.5:** The variation of initial magnetic permeability ($\mu_i$) with temperature at two frequencies.

The permeability at room temperature as a function of Zn and Zr content is shown in ***Fig.6*** for both Zr ratios 0.05 and 0.1.

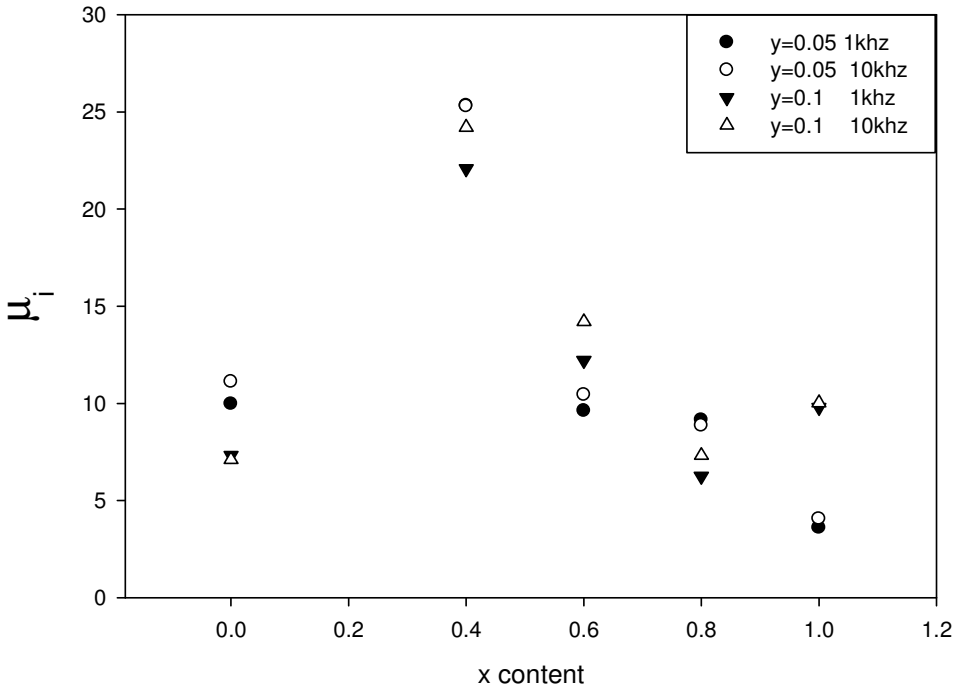


**Fig.6:** The variation of magnetic permeability (μi) with x content for both series at two frequencies.

The increase of $\mu_i$ as Zn content increase up to x=0.4 is attributed to the decrease in magnetic anisotropy field according to Globus relation [27]:

$$\mu_i = \frac{M_s^2 D}{\sqrt{k}}$$

where K is anisotropy constant,

D is the average grain size and

$M_s$ is the saturation magnetization.

About x=0.4, the permeability decrease due to the decrease of saturation magnetization $M_s$. The two compotation factors affect the permeability are the magnetic anisotropy and saturation magnetization.

Noticeable (Mark able) hump appear in all samples near Curie temperature which indicate the presence of single phase structure. After the hump, the $\mu_i$ decrease sharply and reach to very small value near zero due to the transformation from ferromagnetic to paramagnetic. The presence of hump is due to the fast decrease in permeability than the

saturation magnetization. The fast decrease in initial permeability $\mu_i$ at $T_c$ is a good reason to be a very strong candidate for magnetic switch devices.

The Curie temperature decrease by increasing Zn content up to x=0.6 for both ratios of y (0.05 and 0.1) and then increase. It seems to have an opposite relation with saturation magnetization. The Curie temperature obtained from permeability are given in ***Table.4***. Further more it is obvious that, the $\mu_i$ at low Zn content has an inverse relation with the porosity which insure that, the porosity affect and decrease the domain wall motion which consider as the origin of magnetic permeability. The increasing trend of the grain size with increasing Zn content, increase the intergranular pores which leads to the increase of initial permeability up to x=0.4.

The Curie temperature was determined from the interception of extrapolation of linear part of permeability and its interception with temperature axes. The values of $T_c$ and the temperature rate of change of permeability (slope of linear part) are given in ***Table.4***. We can conclude that, the presence of Zn increase the permeability and decrease the Curie temperature, that we can obtain magnetic material with the desired Curie temperature by simply controlling Zn content than $CuFe_2O_4$. This material called magnetic temperature transducer, which have a sudden change in permeability. The higher the slope, the better the devise for controlling temperature.

**Table.4**: The values of $T_c$ (K) and rate of decrease $\mu_i$ with x content.

| y | x | $T_c$ (K) | | Rate of decrease $\mu_i$ ($K^{-1}$) | |
|---|---|---|---|---|---|
| | | 1KHz | 10KHz | 1KHz | 10KHz |
| 0.05 | 0 | 773 | 773 | -0.18 | -0.15 |
| | 0.4 | 456 | 456 | -0.63 | 0.61 |
| | 0.6 | 278 | 278 | -7.02 | -6.83 |
| | 0.8 | 533 | | -0.007 | |
| | 1 | 720 | | -0.18 | |
| 0.1 | 0 | 724 | 735 | -0.14 | -0.19 |
| | 0.4 | 340 | 340 | -0.35 | -0.32 |
| | 0.6 | 224 | 224 | -0.62 | 0.58 |
| | 0.8 | 544 | | -0.01 | |
| | 1 | 683 | | -0.14 | |

Moreover, it was found that, the presence of Zr gives rise to further decrease in permeability and Curie temperature, which make this material very sensitive to thermal

change. The decrease in Curie temperature may be due to the decrease in A-B exchange interaction, which reduce the magnetization and consequently Curie temperature.

From the above discussion, we can say that our samples are suitable for magnetic temperature sensors and devices for temperature controller.

## 3.1 Low Field Hysteresis Loop:

***Fig.7.*** shows the magnetic hysteresis loop for $CuFe_2O_4$ doped with Zn at different ratios of Zr (0.05 and 0.1). The material exhibit typical magnetic hysteresis loop of soft ferrite which indicate that, it is magnetically ordered at low Zn content. At higher Zn contents (x=0.6, 0.8 and 1) the material behave as super paramagnetic material without any saturation $M_s$ and very small coercivity around zero. This behavior is attributed to the very small crystalline size (around 25 nm) at this range. The canting effect at octahedral sites, which arrange the magnetic moments in different directions and not parallel may be the reason for this behavior.

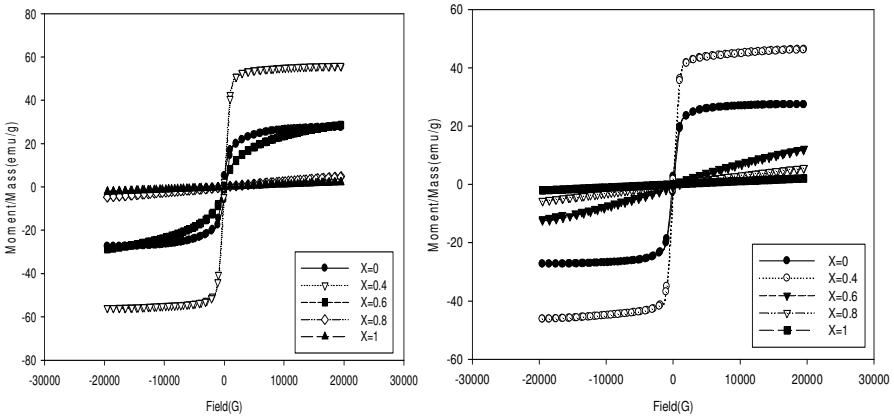


**Fig.7:** Magnetic hysteresis loop for Cu Zn Zr Ferrite when (a) y=0.05 and (b) y=0.1.

The dependence of saturation magnetization on Zn and Zr contents are illustrated in ***Fig.8.*** It was found that, $M_s$ increases up to x=0.4 and then decrease which mean that, there is a limit for the material in ferrimagnetic region and after this limit (x=0.4) the material transfer to super paramagnetic behavior. It is clearly observed that, $M_s$ increases up to x=0.4 according to the resultant sublattice magnetic moment in the basis of Neel's theory model [28].

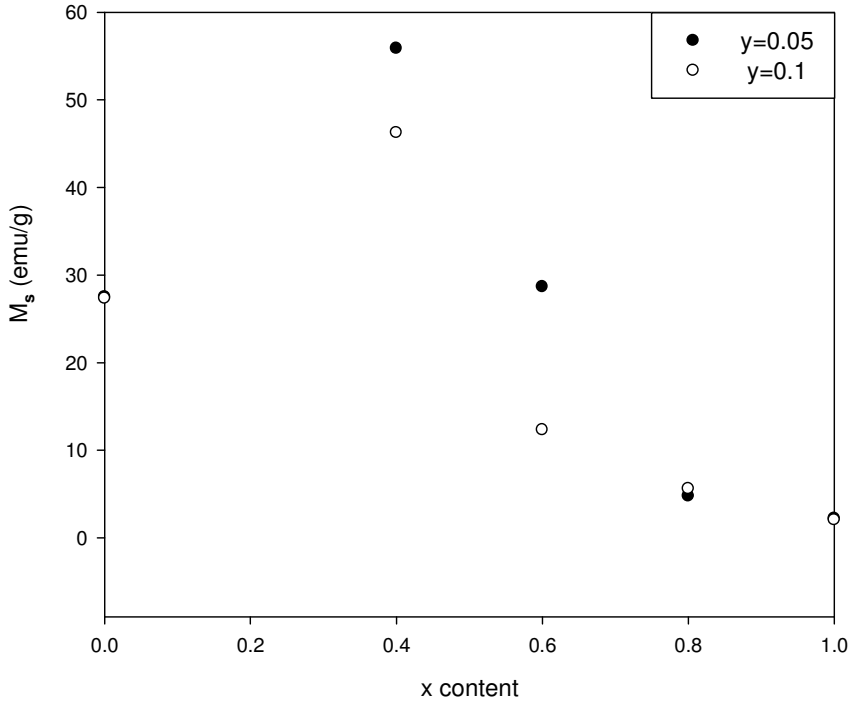


**Fig.8:** The variation of $M_s$ with x content for both series.

The theoretical magnetic moment $\mu_{th}$ is given by $\mu_{th}$ = |M| = $|M_B|$– $|M_A|$. The $\mu_{th}$ depends on the A and B cation distribution which estimated from X-Ray analysis as given before. The general formula for $\mu_{th}$ is given by:

$\mu_{th}$=[1.73(1-x)+5(2x+y)]$\mu_B$ for low Zn content.

$\mu_{th}$=[1.73(1-x)+5(2x+y-2t)]$\mu_B$ for high Zn content.

Where t=0.2y and $\mu_B$ is Bohr magneton.

The magnetic moment depends on the cation distribution among the two sites A and B taking into account that, Zn and Zr are not magnetic materials. The replacement of high spin magnetic moment ions as $Fe^{3+}$ (5 μB) and $Cu^{2+}$ (1.73 μB) by a non magnetic ions $Zn^{2+}$ and $Zr^{4+}$ leads to the weaking of the A and B exchange interaction which is responsible for the decrease of $M_s$ at high Zn content. The experimental magnetic moment can be calculated from the relation [29]:

$$\mu_{exp} = \frac{M_{w.}M_S}{5585}$$

Where $M_s$ is the saturation magnetization obtained from hysteresis loop curve.

The canting at B site means disturbance of the parallel arrangement of spin magnetic moment. The presence of canting spin gives rise to the Yafet-Kittel angle. The Yafet-Kittel angle has been calculated at room temperature using the formula [29]:

$$\mu_{exp} = \mu_B COS\alpha_{Y-K} - \mu_A$$

Where $\alpha_{Y-K}$ is the Yafet-Kittel angle that calculate the strength of A-B and B-B exchange interaction.

The values of $\alpha_{Y-K}$, $\mu_{exp}$ and $\mu_{th}$ for the samples were measured at room temperature are given in ***Table.5***. The $\mu_{exp}$ decrease above x=0.4 indicating the prrobability of non collinearspin at A-Site which is due to the canting between of spin moment. The canting means the disturbance of the parallel magnetic arrangement of spin magnetic moment at B-Site.

**Table.5**: Experimental and theoretical magnetic moments for y=0.05 and 0.1.

| y | x | $\mu_{th}$ | $\mu_{exp}$ | $\alpha_{Y-K}$ |
|---|---|---|---|---|
| 0.05 | 0 | 1.98 | 1.18 | 120 |
| | 0.4 | 5.28 | 2.42 | 90.9 |
| | 0.6 | 6.84 | 1.24 | 92 |
| | 0.8 | 8.49 | 0.20 | 92.1 |
| | 1 | 10.15 | 0.09 | 89.4 |
| 0.1 | 0 | 2.23 | 1.19 | 116 |
| | 0.4 | 5.53 | 1.98 | 90.8 |
| | 0.6 | 6.99 | 0.54 | 93.7 |
| | 0.8 | 10.23 | 0.24 | 89.1 |
| | 1 | 10.3 | 0.09 | 89.4 |

To show the effect of nanostructure on the magnetic properties, a correlation between the crystalline size and saturation magnetization for both ratios was done, and given in ***Fig.9.*** It has observed that, the average crystalline size increases up to x=0.4 and then decrease further. This variation follow nearly the same trend of $M_s$ and $\mu_{exp}$ . Similar results has been reported by [30].

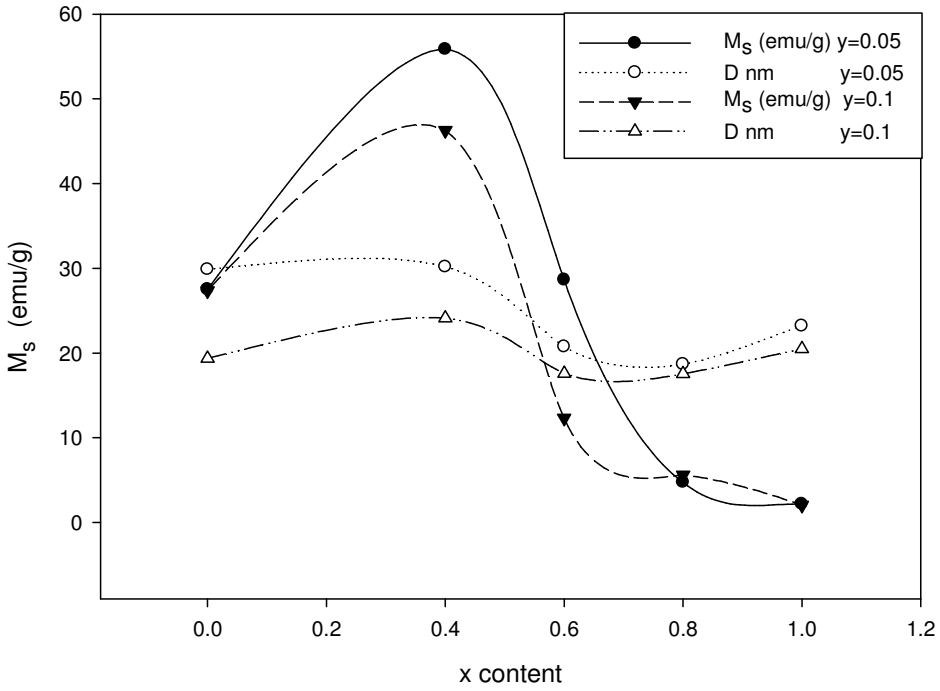


**Fig.9:** The variation of crystalline size and saturation magnetization with x content for both ratios.

The large ionic radius of $Zr^{4+}$ increase the separation between $Fe^{4+}$ ions at B site. Such displacement between $Fe^{3+}$ ions decrease the B-B exchange interaction leading to the decrease of $M_S$ at high Zn and Zr content . The corecivity of the studied samples which can be estimated from H-Loop has high values at low Zn content compared with the very low values at high Zn content, which is an indicator to the super paramagnetic behavior of the material.

***Fig.10***. shows the decrease in $H_c$ with the increase in Zn and Zr content due to the decrease of magnetic crystalline anisotropy[31] according to Browns relation [27]:

$$H_c \geq \frac{2\,k_i}{\mu_\circ\, M_s}$$

Where k is the magnetic anisotropy and

$\mu_\circ$ is the universal constant of permeability for free space.

It is evident that $H_c$ decreases by increasing Zn content while the permeability increase and has highest value at x= 0.4 (Zn content = 0.45 at y=0.05 and 0.5 at y=0.1 ). This behavior can be explained by the previous relation which means that, there is a relation between initial permeability $\mu_i$ and coercivity $H_c$ according to Globus relation [27].

$$\mu_i = \frac{M_s^2 D}{\sqrt{k}}$$

With the increase of Zn content, the formation probability of $Fe^{2+}$ decrease which is the responsible reason for the decrease of anisotropy and leads to the increase of permeability. Thus the decrease in $H_c$ indicates that, the anisotropy constant K is the dominant factor up to x=0.4.

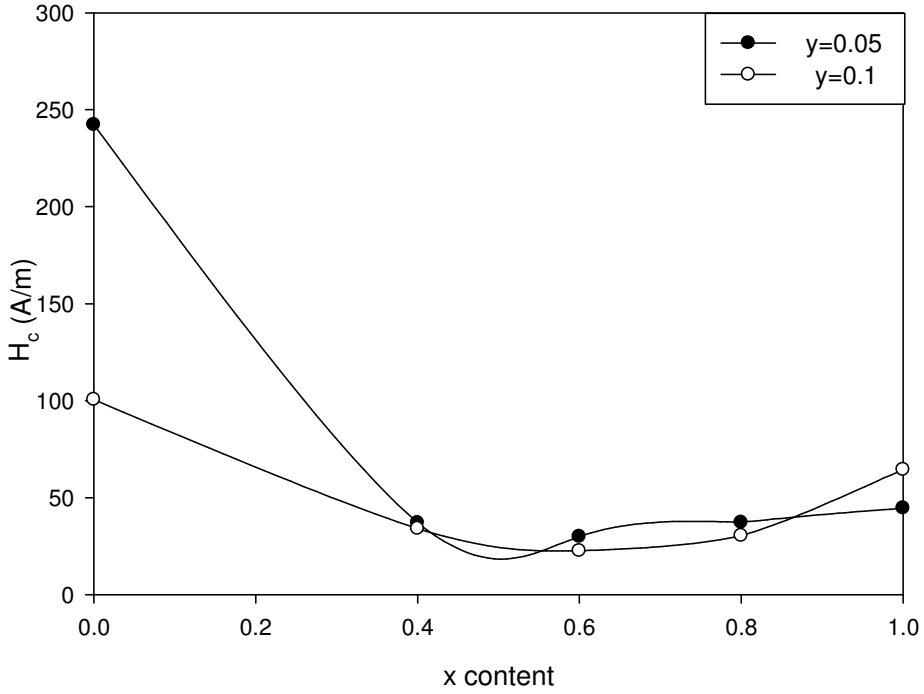


**Fig.10:** The variation of coercivity with x content for both ratios.

When the permeability decrease, the coercivity still decrease also which indicates that, the anisotropy constant K is the dominant factor in this range. The same behavior was observed in the previous study [32, 33]

## 4. Conclusions

Copper Ferrite nanoparticles have been prepared by citrate sol gel technique. X-ray diffraction pattern confirm the formation of single phase structure. The particle size from TEM micrograph and XRD ranged from (17.5-37) nm. Lattice parameter was found to increase by increasing Zn and Zr contents. Grain size was found to increase with increasing Zn content while decrease with Zr content. Initial permeability remains constant with temperature and suddenly drops to near zero at certain temperature called curie temperature

which indicates the formation of single phase of the compounds. The initial permeability has maximum value at x=0.4. The $T_c$ show decreasing trend by increasing Zn and Zr content. Low field hysteresis loop indicates that, the materials were magnetically ordered at low Zn content up to x=0.4. After that, the materials behave as a super paramagnetic without any $M_s$ and very small coercivity $H_c$ around zero.

# References


1. Hassan A, Khan MA, Shahid M, Asghar M, Shakir I, Naseem S, Riaz S, Warsi MF: **Nanocrystalline Zn 1− x Co 0.5 x Ni 0.5 x Fe 2 O 4 ferrites: Fabrication via co-precipitation route with enhanced magnetic and electrical properties**. *Journal of Magnetism and Magnetic Materials* 2015, **393**:56-61.
2. Sattar A, El-Sayed H, Agami W, Ghani A: **Magnetic properties and electrical resistivity of Zr $^{4+} $ substituted Li-Zn ferrite**. *Amer J Appl Sci* 2007, **4**:89-93.
3. Mahmoud K, Hemeda O: **Structural, Magnetic, and Positron Annihilation Characteristics of Zn and Zr-Substituted CuFe2O4 for Magnetic Temperature Controller**. *Journal of Superconductivity and Novel Magnetism* 2016, **29**(10):2669-2679.
4. Rashad M, Mohamed R, Ibrahim M, Ismail L, Abdel-Aal E: **Magnetic and catalytic properties of cubic copper ferrite nanopowders synthesized from secondary resources**. *Advanced Powder Technology* 2012, **23**(3):315-323.
5. Sridhar R, Dachepalli R, K Vijaya K: **Synthesis and characterization of copper substituted nickel nano-ferrites by citrate-gel technique**. *Advances in Materials Physics and Chemistry* 2012, **2012**.
6. Roy P, Nayak BB, Bera J: **Study on electro-magnetic properties of La substituted Ni–Cu–Zn ferrite synthesized by auto-combustion method**. *Journal of Magnetism and Magnetic Materials* 2008, **320**(6):1128-1132.
7. Miclea C, Tanasoiu C, Miclea CF, Spanulescu I, Cioangher M, Miclea CT: **Magnetic Temperature Transducers Made from Copper Based Soft Ferrite.** *Smart Materials & Micro/Nanosystems* 2009, **54**:62-69.
8. Malik H, Mahmood A, Mahmood K, Lodhi MY, Warsi MF, Shakir I, Wahab H, Asghar M, Khan MA: **Influence of cobalt substitution on the magnetic properties of zinc nanocrystals synthesized via micro-emulsion route**. *Ceramics International* 2014, **40**(7):9439-9444.
9. Rashad M, Elsayed E, Moharam M, Abou-Shahba R, Saba A: **Structure and magnetic properties of Ni x Zn 1− x Fe 2 O 4 nanoparticles prepared through co-precipitation method**. *Journal of Alloys and Compounds* 2009, **486**(1):759-767.
10. Priyadharsini P, Pradeep A, Rao PS, Chandrasekaran G: **Structural, spectroscopic and magnetic study of nanocrystalline Ni–Zn ferrites**. *Materials Chemistry and Physics* 2009, **116**(1):207-213.
11. Shahane G, Kumar A, Arora M, Pant R, Lal K: **Synthesis and characterization of Ni–Zn ferrite nanoparticles**. *Journal of Magnetism and Magnetic Materials* 2010, **322**(8):1015-1019.
12. Khan MA, Sabir M, Mahmood A, Asghar M, Mahmood K, Khan MA, Ahmad I, Sher M, Warsi MF: **High frequency dielectric response and magnetic studies of Zn 1− x Tb x Fe 2 O 4 nanocrystalline ferrites synthesized via micro-emulsion technique**. *Journal of Magnetism and Magnetic Materials* 2014, **360**:188-192.
13. Haque MM, Huq M, Hakim M: **Influence of CuO and sintering temperature on the microstructure and magnetic properties of Mg–Cu–Zn ferrites**. *Journal of Magnetism and Magnetic Materials* 2008, **320**(21):2792-2799.
14. Kannan Y, Saravanan R, Srinivasan N, Praveena K, Sadhana K: **Synthesis and characterization of some ferrite nanoparticles prepared by co-precipitation method**. *Journal of Materials Science: Materials in Electronics* 2016, **27**(11):12000-12008.

15. Xia A, Zuo C, Chen L, Jin C, Lv Y: **Hexagonal SrFe 12 O 19 ferrites: hydrothermal synthesis and their sintering properties**. *Journal of Magnetism and Magnetic Materials* 2013, **332**:186-191.
16. Erb U: **Electrodeposited nanocrystals: synthesis, properties and industrial applications**. *Nanostructured Materials* 1995, **6**(5):533-538.
17. O'Connor CJ, Kolesnichenko V, Carpenter E, Sangregorio C, Zhou W, Kumbhar A, Sims J, Agnoli F: **Fabrication and properties of magnetic particles with nanometer dimensions**. *Synthetic Metals* 2001, **122**(3):547-557.
18. Liu T, Wang L, Yang P, Hu B: **Preparation of nanometer CuFe 2 O 4 by auto-combustion and its catalytic activity on the thermal decomposition of ammonium perchlorate**. *Materials Letters* 2008, **62**(24):4056-4058.
19. Das R: **Nanocrystalline ceramics from sucrose process**. *Materials Letters* 2001, **47**(6):344-350.
20. Gubbala S, Nathani H, Koizol K, Misra R: **Magnetic properties of nanocrystalline Ni–Zn, Zn–Mn, and Ni–Mn ferrites synthesized by reverse micelle technique**. *Physica B: Condensed Matter* 2004, **348**(1):317-328.
21. Chang S: **Fabrication Of M-Type Barium Ferrite Nano-Powder With Citrate Sol-Gel Precess**. *IJSTR* 2015, **4**(10):110-112.
22. Yu F, Yuan D, Duan X, Kong L, Shi X, Guo S, Wang L, Cheng X, Wang X: **Citrate sol–gel method to prepare nanoparticles of a piezoelectric crystal material: La 3 Nb 0.5 Ga 5.5 O 14 at low temperature**. *Journal of Alloys and Compounds* 2008, **459**(1):L1-L4.
23. Zahi S, Daud AR, Hashim M: **A comparative study of nickel–zinc ferrites by sol–gel route and solid-state reaction**. *Materials Chemistry and Physics* 2007, **106**(2):452-456.
24. Bahgat M, Farghaly F, Basir SA, Fouad O: **Synthesis, characterization and magnetic properties of microcrystalline lithium cobalt ferrite from spent lithium-ion batteries**. *Journal of materials processing technology* 2007, **183**(1):117-121.
25. Gul I, Abbasi A, Amin F, Anis-ur-Rehman M, Maqsood A: **Structural, magnetic and electrical properties of Co 1− xZnxFe 2 O 4 synthesized by co-precipitation method**. *Journal of Magnetism and Magnetic Materials* 2007, **311**(2):494-499.
26. Sattar A, El-Sayed H, El-Shokrofy K, El-Tabey M: **Study of the dc resistivity and thermoelectric power in Mn-substituted Ni–Zn ferrites**. *Journal of materials science* 2007, **42**(1):149-155.
27. Sattar A, El-Sayed H, Agami W, Ghani A: **Magnetic properties and electrical resistivity of Zr4+ substituted Li-Zn Ferrite**. *Am J Appl Sci* 2007, **4**(2):89-93.
28. Zaki H, Mansour S: **The influence of Ge 4+ and Ti 4+ ions substitution on the magnetic properties of copper ferrite**. *Materials chemistry and physics* 2004, **88**(2):326-332.
29. Topkaya R, Baykal A, Demir A: **Yafet–Kittel-type magnetic order in Zn-substituted cobalt ferrite nanoparticles with uniaxial anisotropy**. *Journal of nanoparticle research* 2013, **15**(1):1-18.
30. Globus A, Pascard H, Cagan V: **Distance between magnetic ions and fundamental properties in ferrites**. *Le Journal de Physique Colloques* 1977, **38**(C1):C1-163-C161-168.
31. Ashiq MN, Saleem S, Malana MA: **Physical, electrical and magnetic properties of nanocrystalline Zr–Ni doped Mn-ferrite synthesized by the co-precipitation method**. *Journal of Alloys and Compounds* 2009, **486**(1):640-644.
32. Yahya N, Aripin MN, Salwani A, A Aziz A, Daud H, Mohd Zaid H, Lim KP, Maarof N: **Synthesis and charaterization of magnesium zinc ferrites as electromagnetic source**. *American Journal of Engineering and Applied Sciences* 2008, **1**(1):53-56.
33. Mazen S, Dawoud H: **Structure and magnetic properties of Li–Cu ferrite**. *physica status solidi (a)* 1999, **172**(2):275-289.